A Polarimetric Antenna-Calibration Method for the Horus Radar based on E-Field Back Projection

David Schvartzman[1,2,3] , José D. Díaz Díaz[4] , Robert D. Palmer[1,2,3] , Dušan Zrnić[5,1,2,3] ,
Caleb Fulton[1,3] , Jorge L. Salazar-Cerreño[1,3] , Patrick Kenworthy[1]

[1]*Advanced Radar Research Center* (ARRC), *The* University *of* Oklahoma
[2]*School of Meteorology*, *The* University *of* Oklahoma
[3]*School of Electrical and Computer Engineering*, *The* University *of* Oklahoma
[4]*Applied Physics Laboratory* (APL), Johns Hopkins University
[5]*National Severe Storms Laboratory*, NOAA/OAR

Abstract—**Phased Array Radar (PAR) technology can provide tailored, high-quality meteorological observations and is rapidly rising as a candidate for future weather radars. To conduct precise measurements of polarimetric weather variables, it is desired that the radar transmits and receives linearly polarized horizontal (H) and vertical (V) fields through beams well matched in gain and shape at every scanning direction. These characteristics are difficult to achieve because the radiation patterns of phased array antennas inherently depend on polarization, beam shape, and gain in the intended pointing direction. Polarimetric array calibration is critical to produce symmetric and matched co-polar antenna patterns at the two polarizations. In this paper, we present a new polarimetric antenna calibration procedure for the all-digital Horus radar based on holographic back projection of electric fields. Near-field Horus measurements are back-projected onto the plane of the array to derive the co-polar magnitude and phase of the H/V fields radiated by each antenna element. Digital calibration parameters are derived from back-projected fields to compensate for excitation differences and produce uniform radiation at the plane of the array. Preliminary results show that through digital calibration based on back-projected fields, co-polar H and V beam matching can be considerably improved. This naturally improves polarimetric measurement accuracy of the Horus radar by mitigating antenna-induced biases in meteorological estimates.**

Index Terms—**phased array radar, radar calibration, polarimetric radar, digital radar, weather radar**

I. Introduction

Phased Array Radar (PAR) technology is being considered for future weather radars because it can provide tailored, high-quality meteorological observations, and thus advance the understanding of atmospheric phenomena [1], [2] while improving warnings and nowcasts. This technology must be integrated with dual-polarization capability, which has become essential for weather radar observations. It involves the transmission and reception of electromagnetic waves in both Horizontal (H) and Vertical (V) polarizations, which are used to estimate spectral moments and polarimetric variables of storms. In the Simultaneous Transmit Simultaneous Receive (STSR) mode, adopted by most operational and research weather radars worldwide, the H- and V-polarized waves are transmitted simultaneously to estimate polarimetric variables.

However, producing accurate polarimetric weather measurements with PARs in STSR is challenging due to the biases induced by the co- and cross-polar antenna patterns when the beam is pointed off broadside [3], [4].

The S-Band mobile polarimetric all-digital Horus radar system is being developed by the Advanced Radar Research Center (ARRC), at the University of Oklahoma (OU), with funding from the National Oceanic and Atmospheric Administration (NOAA). The goal is to produce rapid-update polarimetric observations of meteorological events [5]. The Horus radar system has been integrated and initial deployments for polarimetric weather measurements are being conducted. Considering that the polarimetric performance of a PAR system is largely dictated by the calibration of its far-field radiation patterns, herein we propose a new method for polarimetric PAR calibration to complement the alignment work discussed in the companion paper [6]. Herein, we specifically investigate the holographic back-projection method, that uses near-field measurements to derive electric-field amplitudes and phases radiated by each antenna element. Then, we apply a compensation method to produce uniform aligned excitations that create a symmetric, well-matched H/V far-field radiation patterns.

This paper is organized as follows. In Section II, we present the Horus radar and its design specifications. In Section III, we describe the near-field planar scanner that measures the Horus antenna, and the near-field to far-field transformation procedure. In Section IV, we introduce the back-projection method and provide results from actual Horus near-field measurements. In Section V we discuss the application of this method to improve PAR polarimetric calibration. A summary of the work is in Section VI.

II. The All-Digital Horus PAR

NOAA is exploring digital radar technology [7] and has funded the ARRC to develop an all-digital PAR demonstrator. The mobile Horus radar, shown in the right panel of Fig. 1, is an S-band *engineering* demonstrator under development that

will be completed in 2022 [5], [8]. Its goal is to mitigate risks associated with all-digital phased array architectures and to demonstrate its advanced capabilities. Therefore, it is limited in size and has a 4.5° beamwidth suitable to show functionality and overall scalability, rather than atmospheric research. Element-level waveform and polarization flexibility, imaging, control/calibration methods, and power levels are consistent *by design* with a full-scale system.

An all-digital, dual-polarized array panel defined as an 8×8 mechanical and electrical subarray (middle panel of Fig. 1) is the primary building block. The tube-based frame around the panel provides mechanical support as well as conduit for liquid cooling. The "OctoBlades", eight per panel, house all radar electronics and slide into the panel frame to connect: a) the liquid cooling system, b) the backplane, and c) the antenna array via blind-mate connectors that pass through cutouts in the backplane. The OctoBlades are the heart of the overall digital implementation (left side of Fig. 1). Each panel has a centralized module, the SuperBlade, to support the active electronic components. This module also works with the panel's analog backplane in distributing DC power, local oscillator signal, and a reference clock to each of the OctoBlades. Operating with wideband waveforms from 2.7–3.1 GHz (switchable from dwell-to-dwell), the aperture-coupled, stacked-patch elements provide high polarimetric isolation (better than -45 dB cross-polarization suppression after calibration) [9]. By digitizing at the element level, we have shown that polarimetric calibration of the radar hardware can be robustly accomplished [7].

III. Near-Field Measurements

One antenna panel of the Horus array was fully populated with electronics that make up the transmit and receive signal paths, and was assembled in a near-field chamber for testing (Fig. 2). This setup enables operating the panel as a radar (albeit with a small aperture) to test its performance in the STSR mode for dual-polarization measurements. The near-field scanner is comprised of two motorized Velmex BiSlide assemblies, one Velmex VXM Stepper Motor Controller, an S-band open-ended rectangular waveguide probe (OEWP), a Newport "optical breadboard" base, and RF absorber. These featu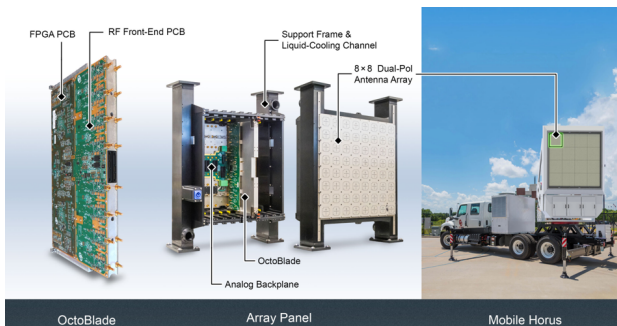res allow measurement of antenna patterns in the H and V polarizations. Two-axis motion is achieved by controlling one stepper motor per axis. The motor controller takes in formatted commands and pulses the stepper motors to achieve the desired movements. The S-band OEWP is mounted to the near-field scanner. The probe is covered with a collar of RF absorber. The near-field scanner is designed so that the system's (0,0) position is in the exact geometric center of the array face.

Our near-field calibration uses a park-and-probe technique to measure amplitude and phase at each channel, generate and apply alignment weights, and then verify the resulting alignment. A full set of transmit patterns requires four separate data collections, one for each combination of array polarization and OEWP orientation (0° or 90°). Although the panel hardware is capable of dual-polarized transmit operation, the OEWP is linearly polarized. Therefore it is impossible to separate the H- from the V transmit response if transmitting both polarizations. Receive patterns can be collected with only two data sets. The panel hardware can receive both polarizations simultaneously and feed back the data separately. Multiple beam angles can be collected simultaneously on RX. Up to 16 beams can be formed at regular intervals.

A. Near-field Samples and Far-Field Transformation

Near-field data was acquired for all 64 channels with both polarizations setting up the OEWP in the transmit and the Horus 8×8 in the receive mode. Figs. 3 and 4 show the measured co- and cross-polar near-field patterns for the H-polarization in the array. Note that the patch locations in the panel are shown for reference using white contour lines.

Determining the far-field radiation patterns of an antenna from near-field measurements requires a mathematical transformation and a correction for the characteristics of the measuring probe. For convenience, we now summarize the mathematical expressions listed in [10] to transform the near-field measurements into far-field radiation patterns.

Fig. 1. The Horus mobile radar, including the OctoBlade and all-digital array panel.

Fully populated Horus panel
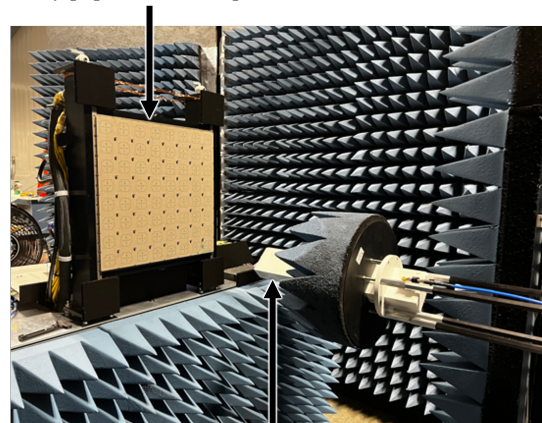
Open-ended rectangular
waveguide S-band probe

Fig. 2. Near-field scanner setup to fully characterize the H and V antenna patterns of the Horus system.

2

|E_x| @ P_d = 334.01 mm [dB]
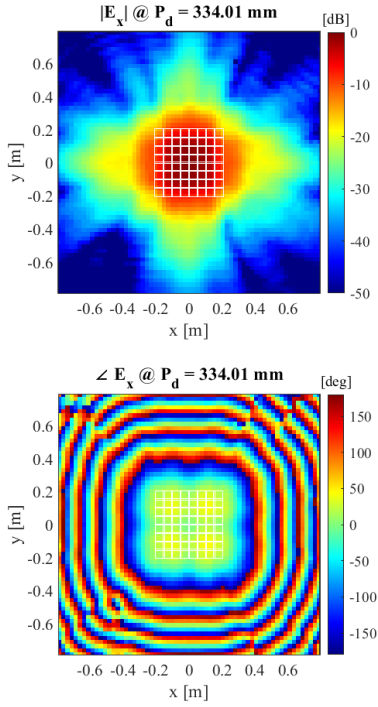
∠E_x @ P_d = 334.01 mm [deg]

Fig. 3. Co-polar planar near-field measurements of the H polarization sampled at 3λ from the Horus antenna panel (top) E-field intensity, and (bottom) phase.

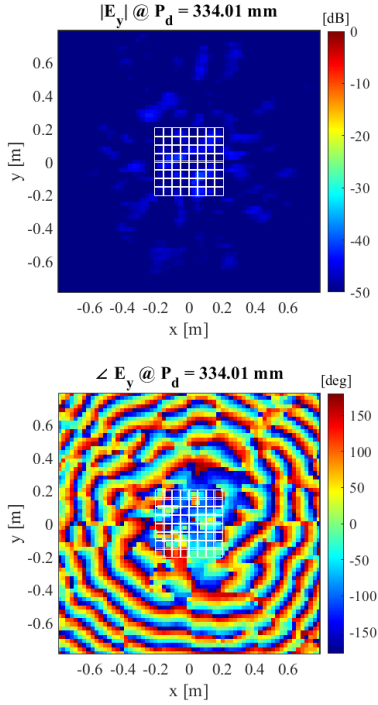|E_y| @ P_d = 334.01 mm [dB]

∠E_y @ P_d = 334.01 mm [deg]

Fig. 4. Same as Fig. 3, but for cross polarization.

Near-field and far-field patterns are Fourier transform pairs [10]. First, assume the measured near-field samples are represented by,

$$E_{xa}(x, y, z = 0) =$$
$$\frac{1}{4\pi^2} \int\limits_{-\infty}^{+\infty} \int\limits_{-\infty}^{+\infty} f_x(k_x, k_y) \ e^{-j(k_x x + k_y y)} \ dk_x dk_y, \qquad (1)$$

where $E_{xa}(x, y, z = 0)$ is the measured electric near-field in the x direction (assumed to be parallel to the ground) sampled in the xy plane parallel to the antenna under test (AUT) at the location of the probe ($z = 0$); $f_x(k_x, k_y)$ represents the plane wave spectrum of the field, and k_x and k_y are the spatial wavenumbers (see eqs. 17-13 a and b in [10]). Similarly, the y component of the near E-field can be represented by,

$$E_{ya}(x, y, z = 0) =$$
$$\frac{1}{4\pi^2} \int\limits_{-\infty}^{+\infty} \int\limits_{-\infty}^{+\infty} f_y(k_x, k_y) \ e^{-j(k_x x + k_y y)} \ dk_x dk_y. \qquad (2)$$

The x and y components of the plane wave spectrum, $f_x(k_x, k_y)$ and $f_y(k_x, k_y)$, are determined from the measured near-zone E-fields using the Fourier transforms of (1) and (2) [10],

$$f_x(k_x, k_y) =$$
$$\int\limits_{-b/2}^{+b/2} \int\limits_{-a/2}^{+a/2} E_{xa}(x', y', z' = 0) \ e^{j(k_x x' + k_y y')} dx' dy', \qquad (3a)$$

$$f_y(k_x, k_y) =$$
$$\int\limits_{-b/2}^{+b/2} \int\limits_{-a/2}^{+a/2} E_{ya}(x', y', z' = 0) \ e^{j(k_x x' + k_y y')} dx' dy', \qquad (3b)$$

where a and b are the width and height of the measuring plane.

The far-field pattern of the antenna in the antenna-relative spherical coordinate system θ, ϕ, can be expressed in terms of the plane wave spectrum equation (3a) and (3b) as

$$E_\theta(R, \theta, \phi) \simeq j \frac{ke^{-jkR}}{2\pi R} (f_x \cos\phi + f_y \sin\phi), \qquad (4)$$

$$E_\phi(R, \theta, \phi) \simeq j \frac{ke^{-jkR}}{2\pi R} \cos\theta(-f_x \sin\phi + f_y \cos\phi), \qquad (5)$$

where R is the range where the far-field radiation pattern is estimated (i.e., $R > 2D^2/\lambda$) and k is the wave number $2\pi/\lambda$. This transformation is applied to the collected near-field samples.
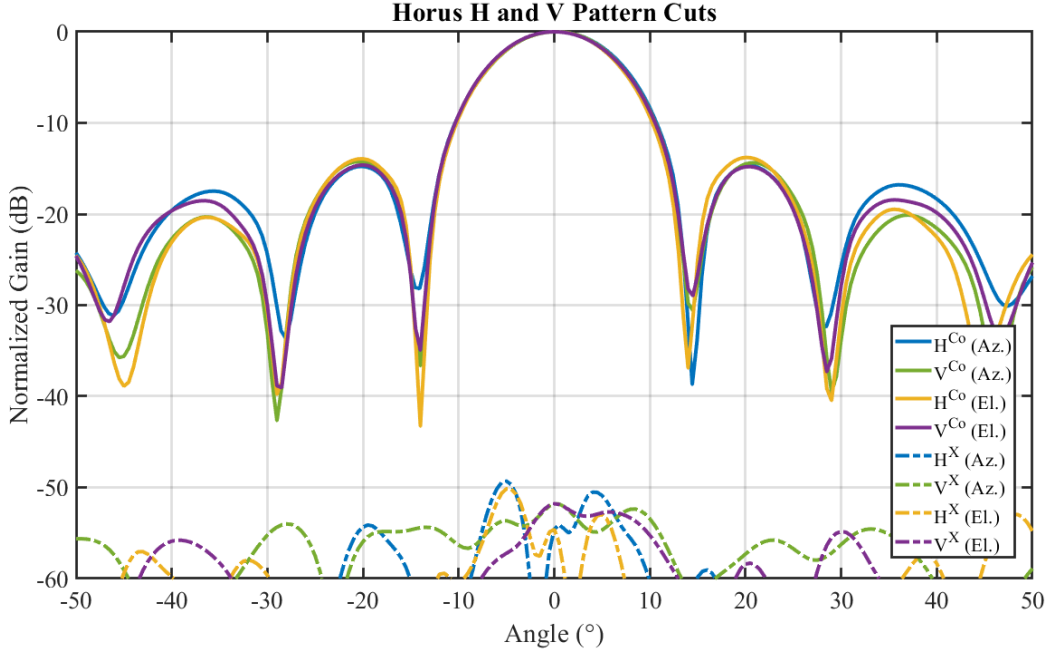
3

Fig. 5. Far-field probe-corrected azimuth and elevation antenna pattern cuts derived using the near-field to far-field transformation.

B. Probe Correction

The far-field radiation patterns acquired through a near-field measurement requires a correction to account for the interaction between the AUT and the measuring probe. This interaction is especially important to the cross-polarized radiation outside of the principal planes. The compensated far-field radiation patterns E_p and E_c shown in this work are given by [11],

$$E_p = \frac{E_{pp,2}E_{pu} - E_{cp,1}E_{cu}}{E_{pp,1}E_{pp,2} - E_{cp,1}E_{cp,2}} \tag{6}$$

$$E_c = \frac{-E_{cp,2}E_{pu} + E_{pp,1}E_{cu}}{E_{pp,1}E_{pp,2} - E_{cp,1}E_{cp,2}} \tag{7}$$

where the subscripts "pp" and "cp" refer to the co-polarized and cross-polarized responses of the probe, "pu" and "cu" to the uncompensated far-field radiation patterns of the AUT, and "1" and "2" to the alignment of the probe with respect to the measured fields. Notice that only one set of co- and cross-polarization patterns are required for the probes. This is due to the $90°$ rotation between probe 1 and probe 2 (i.e., $E_{pp,2} = E_{pp,1}(\phi + 90°)$). The probe electric fields were generated using the dimensions of the OEWP employed in the measurements. The electric fields are found from the closed-form solutions of a slot in an infinite ground derived through spectral techniques [12]. Once these fields are acquired, their corresponding co- and cross-polarization components are estimated and introduced as corrections in (6) and (7). Equations (1) through (5) are applied to the Horus vertical and horizontal near-field measurements, then (6) and (7) are used to compensate for the measuring probe using

the fields of the OEWP. It is in this way that the far-field radiation patterns of this 8×8 array are obtained (i.e., one Horus panel). Normalized cuts of the H and V far-field patterns in the azimuth and elevation planes are presented in Fig. 5.

A qualitative comparison of these patterns indicates excellent mainlobe alignment between the H and V polarizations up to about -20 dB (i.e., $-12.5° \leq \theta \leq 12.5°$). The sidelobe structure for each polarization appears to be symmetric about the mainlobe for the horizontal and vertical cuts. A small difference (≤ 0.7 dB) is observed between peak sidelobe levels in the H and V patterns. This may be caused by finite array effects such as diffraction and mutual coupling [13]. Similarly, the diagonal plane cuts show well matched H and V mainlobes (up to about -20 dB), but sidelobe levels are lower (as expected) due to the rectangular antenna geometry.

IV. BACK-PROJECTION METHOD

The expressions (1) through (5) are applied to the Horus near-field measurements using a negative range r. This range is equal to the distance from the measuring probe to the antenna, such that fields are projected back to the plane of the array. Note that the probe position has to be estimated accurately in 3D space for the holographic back-projection method to work. Further, near-field sampling should be aligned with the center of each element in a uniform grid.

Back-projected E-field magnitudes and phases for the co- and cross-polar H patterns are shown in Figs. 6 and 7. As in Figs. 3 and 4, element locations are delineated with white contour lines. A qualitative analysis of the top panel in Fig. 6 indicates that most of the energy from the measured fields is back-projected on top of the element locations in the
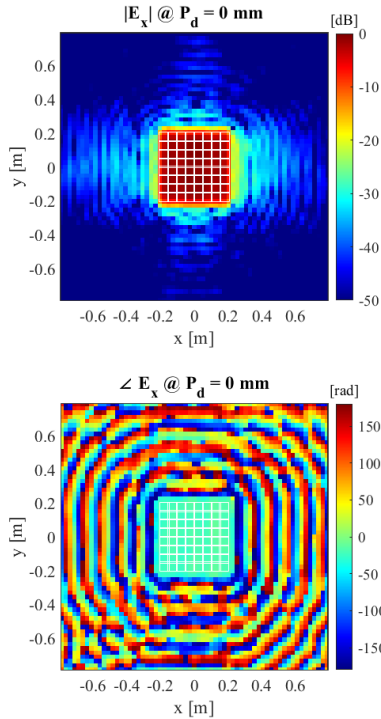
4

Fig. 6. Back-projected copolar H fields on the antenna plane (top) intensity, (bottom) phase.

Fig. 7. Back-projected cross-polar H fields on the antenna plane (top) intensity, (bottom) phase.

array, with well defined power-level transitions (i.e., ~0 dB to ~-20 dB) right along the edges of the panel. Apparent diffraction fields can be observed propagating outwards around the panel. These seem to be particularly stronger in the x direction, aligned with the wave polarization being measured (H). Similarly, back-projected phases shown in the bottom panel of Fig. 6 appear to be close to 0° on the elements. Note that these are raw phase estimates, wrapping in the ±180° interval. Cross-polar field back-projections in Fig. 4 show higher intensity values around the edges of the panel (and especially in the corners), and a non-smooth phase field across the panel.

We propose using back-projected fields (H and V) to perform polarimetric array calibration. That is, since the sampled near-fields capture most of the electric-field energy radiated, we argue that calibration based on back-projected fields can accurately compensate for element-level excitation differences in magnitude and phase. Preliminary results and a discussion on the advantages of this method are discussed next.

V. POLARIMETRIC CALIBRATION

We use the electric-field measurements back-projected on to the plane of the array for polarimetric calibration. To this end, the x and y back-projected fields estimated at the physical location of the antenna elements are extracted. The co-polar, back-projected fields for H and V are shown in Fig. 8. In the co-polar H intensity and phase fields, the standard deviations are 0.47 dB and 3.67° across all 64 elements. Similarly for
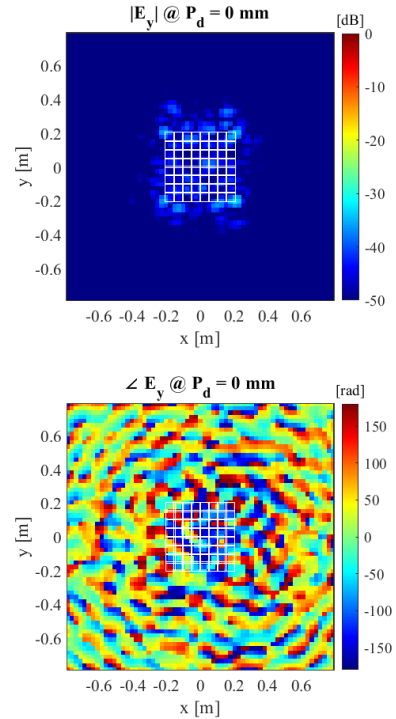
the co-polar V fields, the standard deviations are 0.53 dB and 3.12° across all 64 elements. These variations are due to several practical effects, mainly controlled by amplifier stability in saturation and field diffraction around the array.

We use the linear ratio of co-polar H and V beam patterns as a metric to evaluate polarimetric calibration. It quantifies how well the H and V beams are matched at broadside. Equivalently, one can think of it as the difference of co-polar patterns in dB, presented in Fig. 9 where the dotted black line represents the -3 dB beamwidth of the H pattern. Because the design of the microstrip patch antennas is symmetric, one would expect the far field beams at the H and V polarizations to be relatively well matched. However, due to the calibration and finite array effects, coupled with practical fabrication imperfections, there are differences in the co-polar patterns. These can introduce significant biases in the polarimetric variables, especially as the beam is steered off broadside. Nevertheless, we only investigate the use of back-projection calibration for the broadside beams in this paper and leave the off-broadside evaluation for future work.

Ideally, the magnitude and phase of fields radiated by each element should be 0 dB (normalized) and 0° when forming a beam at broadside. Using the back-projected fields, we derive a set of magnitude and phase weights such that the back-projected fields are equalized (i.e., 0 dB magnitudes and 0° phases). These small calibration corrections are then applied to the fields on the antenna elements and the corrected fields

(including radiation outside of the panel) are projected forward using the traditional near-field to far-field transformation described in Section III. The linear ratio of co-polar H and V beam patterns is derived using the corrected fields and is presented in Fig. 10.

A qualitative comparison of co-polar pattern differences in Figs. 9 and 10 indicates that H and V beam matching is significantly improved. That is, comparing the values inside the -3 dB beamwidths (dotted black lines), it can be seen that differences are close to 0 after the back-projection calibration. Nevertheless, some assumptions are made when emulating the back-projection calibration method here. First, it is likely that the response of the array electronics (specially amplifiers) will not be perfectly linear when applying the back-projection correction values at the element level. Achieving a high level of beam matching would likely entail an iterative back-projection calibration following a "hardware-in-the-loop" type approach. Second, the patterns derived here are based on applying back-projection corrections at the element level and re-projecting the fields forward, which omit diffraction changes. Considering that the back-projection correction values are small, we would expect relatively minor changes in diffraction fields when re-measuring patterns. These would also be accounted for in the iterative process discussed. Lastly, considering magnitude and phase noise in the array, it is likely that back-projection calibration would not result in numerically precise calibration but rather overall statistically accurate (assuming uncorrelated noise). Since the Horus array has 16-bit digital-to-analog converters at the front end before the antenna, we expect noise levels to be small. With these considerations in mind, we believe the back-projection calibration method could be used to achieve high fidelity calibration weights for Horus.
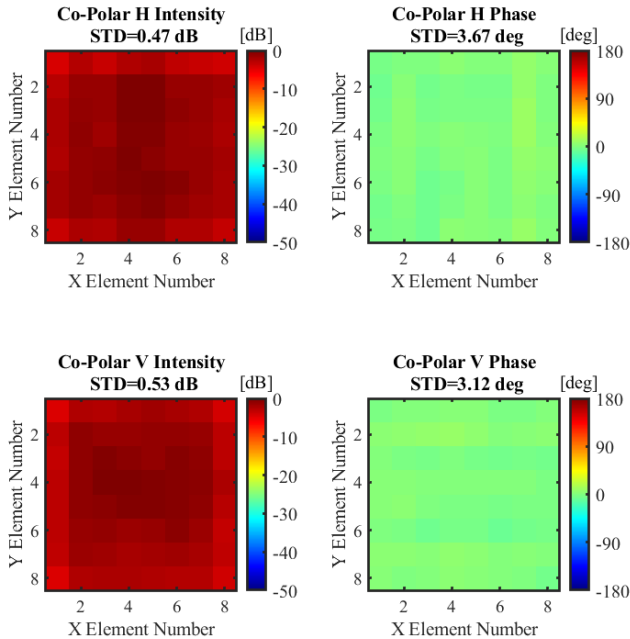

Fig. 8. Magnitude and phase of copolar fields back-projected on the array plane (top) H (bottom) V.
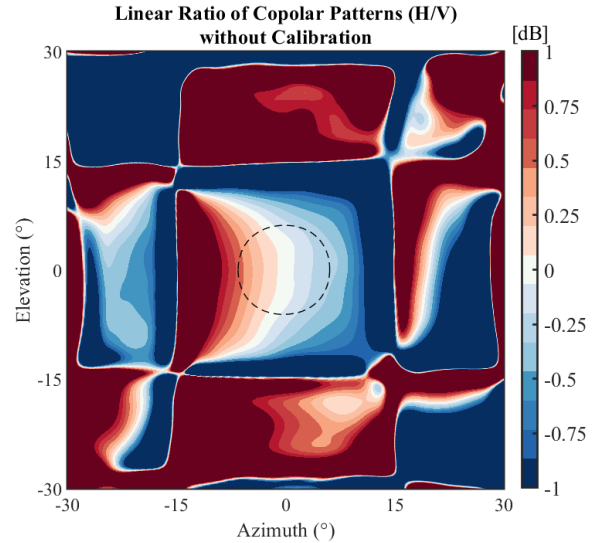

Fig. 9. Difference in measured Horus H and V beam patterns (H - V in dB) without back-projection calibration. This metric quantifies how well the H and V beams are matched at broadside.
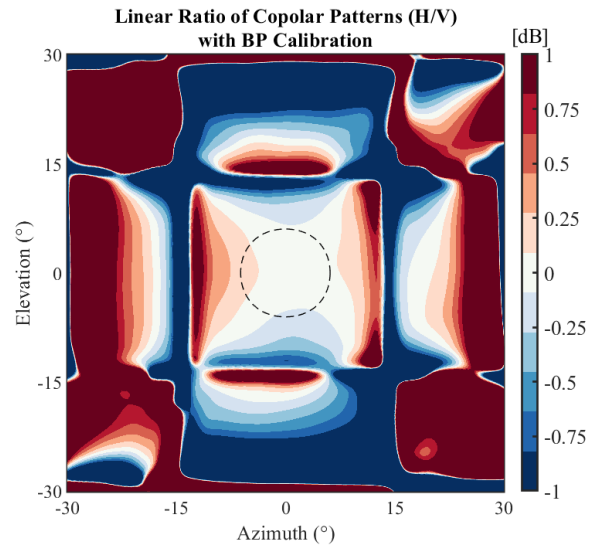

Fig. 10. Similar to 9, but after applying the back-projection calibration method.

VI. CONCLUSION

This paper presents a potential new calibration method for the all-digital Horus polarimetric phased array radar. Horus is an all-digital, polarimetric, S-band phased array radar developed at the ARRC with support from NOAA. The Horus antenna aperture is composed of a 5×5 arrangement of panels (of which not all are active), each with 8×8 antenna elements. With 1024 active elements in total, this proof-of-concept all digital system will have a 3-dB beamwidth of $4.5°$. The Horus radar system has been integrated and initial deployments for polarimetric weather measurements are being conducted.

6

The proposed back-projection calibration method requires a planar near field scanner with enough range to scan a plane with a difference between the maximum and minimum signal that is greater than 40 dB, and with the capability to measure cross-polarization fields. With the near-field measurements, the samples are projected back on to the array plane to get the electric-field intensities and phases of each element. Those are used to derive calibration coefficients, such that the field intensities and phases are uniform. Then fields are projected to far field to remove the effects from the probe. The linear ratio of H and V (their difference in dB) is used as a metric to evaluate co-polar H/V beam matching. The back-projection calibration method digitally corrects the magnitude and phase variations across the array (for each element) to equalize radiated fields. As shown in Section V, this results in significantly improved H/V beam matching, after taking the fields corrected at the aperture to the far field. It is important to note the performance relies on linearity of the amplifiers operating near saturation, array stability, and the precision of the element-level excitations. Although the back-projection calibration is only emulated here, we plan to test it with the actual Horus 8×8 panel in the near future.

Some potential advantages of this method include the possibility to calibrate a polarimetric array without the need for an external far-field probe, fast calibration over large bandwidths, and higher accuracy in H/V beam matching. Polarimetric calibration can be conducted measuring far-field patterns to digitally compensate for mismatches and gain/phase imbalances. However, deploying a far-field measurement probe and getting uncontaminated samples in the presence of multi-path and external interference can be challenging. Large bandwidths could be measured by sweeping a desired frequency range while collecting near-field samples and independently post-processing each frequency to produce back-projection calibration lookup tables. Lastly, if most of the electric-field energy is appropriately sampled in an uncontaminated near-field environment, and the array is sufficiently stable, the corrections derived could provide high levels of H/V beam matching. This naturally improves measurements accuracy by mitigating antenna-induced biases in meteorological estimates.

REFERENCES

[1] D. S. Zrnic *et al.*, "Agile-Beam Phased Array Radar for Weather Observations," *Bulletin of the American Meteorological Society*, vol. 88, no. 11, pp. 1753–1766, 11 2007.

[2] R. Palmer, D. Bodine, P. Kollias, D. Schvartzman, D. Zrnić, P. Kirstetter, G. Zhang, T.-Y. Yu, M. Kumjian, B. Cheong, S. Collis, S. Frasier, C. Fulton, K. Hondl, J. Kurdzo, T. Ushio, A. Rowe, J. Salazar-Cerreño, S. Torres, M. Weber, and M. Yeary, "A primer on phased array radar technology for the atmospheric sciences," *Bulletin of the American Meteorological Society*, 2022. [Online]. Available: https://journals.ametsoc.org/view/journals/bams/aop/BAMS-D-21-0172.1/BAMS-D-21-0172.1.xml

[3] J. D. Díaz, J. L. Salazar-Cerreno, J. A. Ortiz, N. A. Aboserwal, R. M. Lebrón, C. Fulton, and R. D. Palmer, "A cross-stacked radiating antenna with enhanced scanning performance for digital beamforming multifunction phased-array radars," *IEEE Transactions on Antennas and Propagation*, vol. 66, no. 10, pp. 5258–5267, 2018.

[4] I. Ivić, C. Curtis, E. Forren, R. Mendoza, D. Schvartzman, S. Torres, D. J. Wasielewski, and F. A. Zahrai, "An overview of weather calibration for the advanced technology demonstrator," in *2019 IEEE International Symposium on Phased Array System Technology (PAST)*, Oct 2019, pp. 1–7.

[5] R. D. Palmer, C. J. Fulton, J. Salazar, H. Sigmarsson, and M. Yeary, "The "Horus" radar—an all-digital polarimetric phased array radar for multi-mission surveillance," in *99th American Meteorological Society Annual Meeting*. AMS, 2019.

[6] C. Fulton, S. Garner, P. Kenworthy, D. T. J. Lujan, and M. Yeary, "Mutual Coupling-Based Calibration for the Horus Digital Phased Array Radar," in *2022 IEEE International Symposium on Phased Array Systems and Technology*, 2022.

[7] C. Fulton *et al.*, "Digital Phased Arrays: Challenges and Opportunities," *Proceedings of the IEEE*, vol. 104, no. 3, pp. 487–503, 2016.

[8] M. Yeary, R. Palmer, C. Fulton, J. Salazar-Cerreno, and H. Sigmarsson, "Preliminary chamber measurements and a status report on the development of an all-digital mobile phased array radar," in *2022 IEEE Radar Conference (RadarConf22)*, 2022, pp. 1–5.

[9] J. D. Díaz, "Ultra-low cross polarization antenna architectures for multi-function planar phased arrays," Ph.D. dissertation, The University of Oklahoma, Norman, OK, USA, 2021, available at https://hdl.handle.net/11244/330113.

[10] C. A. Balanis, *Antenna theory: analysis and design*. John wiley & sons, 2015.

[11] G. F. Masters, "Probe-Correction Coefficients Derived from Near-field Measurements," in *Antenna Measurement Techniques Association Symposium*. AMTA, 1991.

[12] C. A. Balanis, *Antenna Theory: Analysis and Design*, 2nd ed. John Wiley & Sons, 2005.

[13] J. A. Ortiz, "Impact of edge diffraction in dual-polarized phased array antennas," Ph.D. dissertation, The University of Oklahoma, Norman, OK, USA, 2020, available at https://shareok.org/handle/11244/325369.